Available online at www.sciencedirect.com
ScienceDirect
Mechanical Systems and Signal Processing 21 (2007) 2697–2714
Mechanical Systems and Signal Processing
www.elsevier.com/locate/jnlabr/ymssp

Component system identification and state-space model synthesis

Per Sjövall*, Thomas Abrahamsson

Department of Applied Mechanics, Chalmers University of Technology, SE-412 96 Göteborg, Sweden

Received 1 November 2006; received in revised form 9 March 2007; accepted 13 March 2007
Available online 19 March 2007

Abstract

A scheme for synthesis of subsystem state-space models to be used for analysis of dynamic behaviour of built-up structures is presented. Using measurements on each component, subsystem models are identified adopting contemporary system identification methods. The subsystem state-space models are transformed into a coupling form, at which kinematic constraints and equilibrium conditions for the interfaces are introduced. The procedure is applied to a plane frame structure, which is built up of two components. It is found that the non-trivial model order determination constitutes a crucial step in the process. If the model order is incorrect at subsystem level, the synthesized model may radically fail to describe the properties of the built-up structure. It is also found that the identified subsystem models need to satisfy certain physically motivated constraints, e.g. reciprocity and passivity. Different approaches and methods to aid the model order determination and the estimation of physically consistent state-space models at subsystem level are discussed.

Keywords: State-space models; System identification; Modal identification; Experimental modal analysis; Constraints; Component synthesis

1. Introduction

For analysis and prediction of complex built-up mechanical system it is convenient to consider it as an assembly of subsystems. In order to establish an adequate model of such a subsystem, there are different approaches. One straightforward way is to apply the assembly process of the finite element method (FEM) and build the model based on physical knowledge. The physical parameters, i.e. geometry, stiffness, mass etc., are then given more or less accurate values based on knowledge and/or experience. Another approach is to excite the subsystem, measure the response and then apply system identification to get a test data-based system description, see Ljung [1]. A model is identified, based on the excitation and the measured response, that describes the system's input–output behaviour as good as possible. This is sometimes referred to as a black-box modelling technique as it gives no insight of the underlying physics. In fact this approach can be said to be quite opposite to FE modelling, which primarily focus on modelling of the physical properties. Consequently FEM is sometimes referred to as white-box modelling. However, obtained test data may also be considered in

*Corresponding author.
E-mail addresses: per.sjovall@chalmers.se (P. Sjövall), thomas.abrahamsson@chalmers.se (T. Abrahamsson).

0888-3270/$ - see front matter © 2007 Published by Elsevier Ltd.
doi:10.1016/j.ymssp.2007.03.002

FE modelling. This is referred to as grey-box modelling or FE model updating, see Friswell and Mottershead [2], where the physical parameters of the model are calibrated to minimize analysis-to-test deviations.

In this report, a combination of FEM and system identification is studied. The idea is to utilize state-space models of the subsystems, obtained using either system identification or FEM, and then synthesize the models resulting in a model of the total system. For most subsystems only one of these modelling methods is preferable for different reasons. Hence, a method for synthesis of subsystem state-space models provides a possibility to use the most adequate modelling technique for each subsystem.

The problem to synthesize subsystem models to obtain an analysis model for a coupled structure has been a research field since the 1960s and a large number of different methods are available. The methods, usually referred to as dynamic substructuring methods, can be divided into two main parts, component mode synthesis (CMS) and frequency response function (FRF)-based coupling. CMS techniques set out from modal models originating from either FE models, or identified by experimental modal analysis (EMA), see Ewins [3], whereas FRF coupling methods are best suited for purely experimental models. For a review of CMS methods, see for instance Meirovitch [4], Craig [5] or Craig and Kurdila [6]. Compared to CMS, FRF coupling techniques have the advantage to be able to use the measured FRFs directly. Hence, errors induced by modal analysis, e.g. mode truncation, can be eliminated since the influence of high frequency modes is naturally included in the measured response. The basic idea for FRF coupling techniques can be traced back to the book by Bishop and Johnson [7]. There, the equations for the kinematic constraints and equilibrium conditions for FRFs were first introduced. After that the procedures have been extended and refined. Jetmundsen et al. [8] systematically presented a formulation which significantly improves the numerical efficiency. It was shown that the number of required matrix inversions at each frequency line can be reduced from three to one. Thereby, the error amplification caused by ill-conditioned matrix inversions can be decreased. The method was further developed by Liu and Ewins [9], who introduced a possibility to model an elastic joint between the substructures. Other attempts to improve the procedure have been developed by Otte et al. [10] and Lim and Li [11]. They proposed to reduce the error amplification by a singular-value decomposition (SVD) of the FRF matrix and subsequent truncation of the lowest singular values. A generalized FRF coupling technique was formulated by Ren and Beards [12]. With their formulation linearly dependent coordinate pairs, which cause ill-conditioned FRF matrices, can be identified and removed.

The presently addressed method to synthesize state-space models is closely related to the FRF coupling techniques setting out from experimental data. However, instead of coupling measured FRFs directly, substructure state-space models are identified as an intermediate step. The order of the models is given by the user of the identification tool and thus, also this approach has the ability to account for high frequency modes.

In Su and Juang [13], the benefit of applying the system identification routines on substructure level was emphasized. The motivation is simply that it is easier to identify a lower order substructure model than a higher order coupled structure model. They also formulated a procedure for synthesis of state-space models, which has large similarities to the method presented herein.

The paper is organized as follows: in Section 2, the process to identify a subsystem state-space model from experimental data is described. In Section 3, a scheme for synthesis of subsystem state-space models is presented. The numerical example in Section 4 and the case study in Section 5 illustrates the procedure and critical properties of the identified subsystem models are identified. Finally, in Section 6, some concluding remarks are made.

2. System identification

The inverse problem to estimate a system model from measured input–output data is called system identification. In structural dynamics the term EMA is also commonly used. System identification constitutes a vast research field and several text books are available, e.g. Ljung [1] and Van Overschee and DeMoor [14].

A convenient description of a linear and time-invariant (LTI) dynamic system is the continuous-time state-space form:

$$\dot{x} = Ax + Bu, \tag{1}$$

$$y = Cx + Du. \tag{2}$$

Here x is the n-dimensional state vector with n being the model order, $A \in \mathbb{R}^{n\times n}$, $B \in \mathbb{R}^{n\times m}$, $C \in \mathbb{R}^{p\times n}$ and $D \in \mathbb{R}^{p\times m}$ are parameter matrices, whereas y is the p-dimensional response vector and u the m-dimensional stimuli vector. The corresponding frequency domain equation for stationary harmonic loading is

$$\hat{y} = [C(\mathrm{i}\omega I - A)^{-1}B + D]\hat{u} \stackrel{\text{def}}{=} H(\omega)\hat{u}, \tag{3}$$

where $H(\omega) \in \mathbb{C}^{p\times m}$ is the multivariate frequency domain transfer function, the FRF matrix.

The system identification problem consists of finding estimates of the quadruple $\{A, B, C, D\}$ given measured input–output data $\{u, y\}$ or $\{\hat{u}, \hat{y}\}$. For structural dynamic systems, recently developed subspace-based state-space methods (4SID) are well suited. Both frequency domain methods, see McKelvey et al. [15], and time domain methods, see Viberg [16], exist. These methods have the advantage to be non-iterative, which allow estimation of large models, i.e. models covering a broad frequency spectrum.

Here the focus is twofold. A practical difficulty in all system identification is the model order determination, which is complicated by possible poorly identifiable eigenmodes due to test design and the presence of noise in test data. The model order determination is addressed. Furthermore, identification of models that satisfy basic physical properties of vibrating linear structures is treated. Details regarding subspace methods are outside the scope of this paper.

2.1. Model order determination

The model order n, which is an integer parameter provided by the user, governs the number of modes in the model. In practice when measurements are corrupted with noise, the model order is most often ambiguous. Also in the case with very little noise, the model order may be hard to estimate, as the structure may have adjacent, or even coalescent, eigenfrequencies. A number of tools are available to aid the model order determination, of which a few, suitable for identification using frequency domain data, are discussed next.

Setting out from a measured receptance FRF matrix H_X, different mode indicator functions (MIFs) can be constructed such as the multivariate mode indicator function (MMIF) and the complex mode indicator function (CMIF), see Radeş [17]. The MMIF is defined as the eigenvalues $\lambda_{\mathrm{MMIF}}(\omega)$ of the generalized eigenproblem

$$\Re\{H_X\}^T\Re\{H_X\}Q = \lambda_{\mathrm{MMIF}}(\Re\{H_X\}^T\Re\{H_X\} + \Im\{H_X\}^T\Im\{H_X\})Q, \tag{4}$$

where a local minima of the smallest eigenvalue dropping towards zero indicate an eigenfrequency with low damping. Simultaneous drops of the eigenvalues indicate multiple resonances at the particular frequency. On the other hand, the CMIF is defined by the eigenvalues $\lambda_{\mathrm{CMIF}}(\omega)$ associated with

$$H_X^* H_X Q = \lambda_{\mathrm{CMIF}} Q, \tag{5}$$

where the superscript $*$ denotes the complex-conjugate transpose. Clear peaks of the largest eigenvalue indicate an eigenfrequency and consequently the existence of multiple collocated peaks suggests a multiple resonance. A MIF is generally capable to detect multiple modes for high signal to noise ratio (SNR). However, for low SNR, a MIF may be unable to distinguish a physical mode from a spurious mode introduced by noise.

A more sophisticated, yet simple, tool is the stabilization chart. Several models with increasing model order are identified and the imaginary parts of the poles (the eigenfrequencies) are plotted for each model. A pole that is present at the same frequency for increasing model order is called stable and is presumed to correspond to a physical vibrational mode. Poles that are not stable are then concluded to be unphysical computational modes, i.e. modes that fit the model to the noise. Cauberghe et al. [18] show that by using the complex conjugate of the FRF matrix in the identification an even clearer stabilization chart is obtained. By this simple manipulation it is possible to distinguish physical modes from unphysical computational modes considering the sign of the estimated damping coefficient.

There are cases when an FE model of the tested system could provide useful information for model order determination, i.e. the content of eigenmodes in a specific frequency range. Considering the distribution of eigenfrequencies and the mode shapes a qualitative assessment of the model order can be made. However, one may argue for this to be an incorrect approach: If an FE model is available, why not use it instead of considering experiments? Or, if the purpose of the identified experimental model is to validate an FE model, it

is doubtful to use it in the identification process. Nevertheless, modelling from first principles will increase the qualitative knowledge of the system at hand.

2.2. Low frequency residual modes

In a real situation, measured frequency domain input–output data are seldom available below a certain frequency due to measurement system limitations. Modes at eigenfrequencies below the lowest excitation frequency are here called low frequency residual modes. Accordingly, modes at eigenfrequencies above the highest excitation frequency are called high frequency residual modes. The model's ability to reproduce test data will increase, especially close to the limits of the excitation frequency band, if these residual modes are taken into account in the model.

More important though, in the context of subsystem synthesis, the influence of subsystem low frequency residual modes may be substantial on coupled system level. This is motivated by Rayleigh's theorem, see e.g. Meirovitch [19], which states that if n_c scalar constraints are imposed on a system, the eigenvalues $\bar{\lambda}$ of the modified system are bracketed by those of the initial unconstrained system according to the inequality

$$\lambda_r \leqslant \bar{\lambda} \leqslant \lambda_{r+n_c}. \tag{6}$$

Consequently, the eigenfrequencies of a synthesized model in the frequency range of interest are highly affected by subsystem eigenfrequencies below that frequency range. In particular, if the low frequency residuals are not included in the subsystem models, eigenmodes of the coupled system will be missing in the synthesized model. If the eigenfrequencies of these missing modes lie within the frequency range of interest, the resulting coupled system model will be poor.

The easiest way to include the low frequency residuals is to simply add poles and estimate the corresponding mode shapes using test data. However, as the influence of the residual modes on the component's FRF in the measured frequency range may be small, sometimes almost negligible, the identifiability of the residual mode shapes in the test data can be poor. Nevertheless, the subsystem residual mode shapes are of great importance on synthesized system level. Therefore, we advocate the use of low frequency residual mode shapes calculated from first principles, e.g. by FE modelling.

2.3. Physically consistent models

A structural dynamic LTI system possesses some basic physical properties. Certain MIMO systems, non-gyroscopic and non-circulatory, exhibit reciprocity. Thus, a partition of the FRF matrix corresponding to collocated and co-orientated sensor–actuator pairs should be symmetric in theory. Moreover, if the system is stable with no possible rigid body motion we have that velocity and acceleration responses in statics ($\omega = 0$) are zero. Furthermore, if the excitation is a force and the response consists of velocities and/or displacements the direct throughput matrix D in the state-space model equals the zero matrix. According to Newton's second law of motion, force is proportional to acceleration. To obtain velocity or displacement, force has to be integrated, which implies that the direct throughput vanish. In Sjövall et al. [20] state-space model identification subject to these three types of physically motivated constraints is addressed.

Here two additional physical properties are treated. Consider the static response in terms of displacements due to force excitation, i.e. the static flexibility. Provided that the system has no possible rigid body motion and the response is collocated and co-orientated with the excitation, we must have that the static flexibility matrix is positive definite.

The final basic physical property of mechanical vibrating LTI systems is passivity. The total vibrational power supplied to a passive structure is always non-negative and equals zero only in the theoretical case of an undamped structure, in which there is no energy dissipation. Regarding the mobility FRF matrix of a passive system we have the following result.

Lemma 1 (*Passivity criterion*). *Let* $H(\omega) = H(\omega)^T \in \mathbb{C}^{m\times m}$ *be the mobility FRF matrix of a reciprocal system and* $W(\omega)$ *the supplied power by the loading at the system interface. Then* $W(\omega) \geqslant 0 \Leftrightarrow \Re\{H(\omega)\} \geqslant 0$, $\forall \omega \in \mathbb{R}$.

Proof. Let $\hat{u} \in \mathbb{C}^{m\times 1}$ be the exciting forces and $\hat{v} = H(\omega)\hat{u} \in \mathbb{C}^{m\times 1}$ be the velocity responses collocated and co-orientated with $\hat{u}$. The total supplied power is then

$$W = \Re\left\{\tfrac{1}{2}\hat{u}^*\hat{v}\right\} = \Re\left\{\tfrac{1}{2}\hat{u}^*H\hat{u}\right\}. \tag{7}$$

With $a = \Re\{\hat{u}\} \in \mathbb{R}^{m\times 1}$ and $b = \Im\{\hat{u}\} \in \mathbb{R}^{m\times 1}$, we have

$$W = \tfrac{1}{2}(a^T\Re\{H\}a + b^T\Re\{H\}b). \tag{8}$$

Since a and b can be arbitrarily chosen in $\mathbb{R}^{m\times 1}$, the proof is concluded. □

This is related to the positive real (PR) lemma from systems and control theory, see e.g. Anderson and Vongpanitlerd [21] or Åström and Wittenmark [22]. For systems with no direct throughput, $D = 0$, the following version of the PR lemma is particularly useful, Curtain [23].

Lemma 2 (*PR lemma*). *Given $A \in \mathbb{R}^{n\times n}$, $B \in \mathbb{R}^{n\times m}$ and $C \in \mathbb{R}^{m\times n}$, with all eigenvalues of A in the negative real half-plane and $\{A, B, C\}$ minimal, and $H(\omega) = C(\mathrm{i}\omega I - A)^{-1}B$, the following two statements are equivalent*:

(i) *For $\omega \in \mathbb{R}$,*

$$H(\omega) + H(\omega)^* \geqslant 0. \tag{9}$$

(ii) *There exist a positive definite matrix $P = P^T \in \mathbb{R}^{n\times n}$, i.e. $P > 0$, such that*

$$PA + A^TP \leqslant 0, \tag{10}$$

$$B^TP = C. \tag{11}$$

A proof of the result can be found in Anderson [24]. Note that for reciprocal systems $H(\omega) + H(\omega)^* = 2\Re\{H(\omega)\}$, which connects the PR lemma to the passivity criterion. In particular, the passivity criterion implies that the phase angle of the diagonal elements of the mobility FRF matrix H are bounded to the interval $[-90^\circ, 90^\circ]$.

A physically consistent real parametrization of a stable mechanical vibrating system is

$$\ddot{\eta} + \Xi\dot{\eta} + \Omega^2\eta = \Phi^T u, \tag{12}$$

$$y = \Phi\dot{\eta}, \tag{13}$$

where $\Omega = \mathrm{diag}\{w_1, w_2, \ldots, w_{n/2}\} \geqslant 0$ and $\Xi = \Xi^T \geqslant 0$. This is recognized as the second order equations of motion in the modal coordinates η. For this parametrization the system of second order ODEs can equivalently be written as a system of first order ODEs in state-space form

$$A = \begin{bmatrix} 0 & I \\ -\Omega^2 & -\Xi \end{bmatrix}, \quad B = \begin{bmatrix} 0 \\ \Phi^T \end{bmatrix}, \quad C^T = B. \tag{14}$$

The positive realness of the model parameterized according to Eqs. (14) is easily verified using Lemma 2. From Eq. (11) we conclude that the structure of P need to be

$$P = \begin{bmatrix} P_{11} & 0 \\ 0 & I \end{bmatrix}. \tag{15}$$

Inserting this into the left-hand-side of Eq. (10) we have

$$PA + A^TP = \begin{bmatrix} 0 & P_{11} - \Omega^2 \\ P_{11} - \Omega^2 & -2\Xi \end{bmatrix}, \tag{16}$$

which is negative semi-definite if and only if $P_{11} = \Omega^2$, for which also $P > 0$ provided $\Omega^2 > 0$. Further, the feasibility of the reciprocity and the static response constraints is easily verified considering the frequency

domain version of Eqs. (12) and (13) for stationary harmonic loading,

$$\hat{y} = \mathrm{i}\omega\Phi(-\omega^2 I + \mathrm{i}\omega\Xi + \Omega^2)^{-1}\Phi^T\hat{u} \stackrel{\text{def}}{=} H(\omega)\hat{u}. \tag{17}$$

We see that $H(\omega) = H(\omega)^T$ and $H(0) = 0$ by construction. Furthermore, the static flexibility is $\Phi\Omega^{-2}\Phi^T > 0$ provided that $\Omega = \mathrm{diag}\{w_1, w_2, \ldots, w_{n/2}\} > 0$.

2.4. Constrained model estimation

The process to estimate a physically consistent parametric model from measured input–output data can be regarded as a two-step procedure. System identification, typically adopting a subspace method, followed by a constrained minimization of the transfer function error ε, defined as

$$\varepsilon = \sum_k e_k^* \mathscr{W}_k e_k, \tag{18}$$

where e_k is the residual vector at angular frequency ω_k and $\mathscr{W}_k$ is a symmetric positive definite weighting matrix. The residual vector e_k is defined as

$$e_k = \mathrm{vec}(C(\mathrm{i}\omega_k I - A)^{-1}B - H_{X,k}), \tag{19}$$

where $H_{X,k}$ is the measured FRF matrix at ω_k.

Application of the subspace methods as described in McKelvey et al. [15] and Viberg [16] using measured input–output data provides a model in discrete-time state-space form. A model in continuous-time form may then be obtained via a bilinear transformation, see again McKelvey et al. [15]. The frequency domain subspace methods formulated directly in continuous-time are numerically ill-conditioned and is therefore most often an infeasible approach.

In order to find a physically consistent model according to Eqs. (14), the model identified by a subspace method has to be post-processed. Setting out from the A-matrix as estimated by the subspace method, corresponding Ω^2 and a diagonal version of Ξ of the formulation of Eqs. (14) can be found by applying a similarity transformation, see Alvin and Park [25]. The corresponding transformed versions of C and B will in general not have the structure according to Eqs. (14). However, minimizing the transfer function error ε by optimization of the elements of $\mathrm{diag}\{\Omega^2\}$, $\Xi = \Xi^T$ and Φ gives a physically consistent model provided that the constraints $\Omega^2 > 0$ and $\Xi \geqslant 0$ are satisfied. Unfortunately, this constitutes a quite complicated optimization problem due to the constraint characteristics.

A simplification is to assume that the damping is of Caughey type, normally considered to be a good approximation for lightly damped structures with separated eigenfrequencies. Then, we can use the A-matrix as estimated by the subspace method, provided that it is stable, with its corresponding Ω^2 and diagonal Ξ and parameterize the modal participation matrix Φ only. Because the physical consistency if this parametrization is guaranteed by construction, the optimization problem is unconstrained.

3. Component synthesis

Consider two state-space models describing the mechanical components I and II,

$$\dot{x}^i = A^i x^i + B^i u^i, \tag{20}$$

$$y^i = C^i x^i, \tag{21}$$

where $i = \mathrm{I}, \mathrm{II}$. The excitation vector u^i contain external forces and the response vector y^i displacements and/or velocities and they are partitioned with respect to coupling degrees of freedoms (DOFs), subscript c, and internal body DOFs, subscript b,

$$y^i = \begin{Bmatrix} y_c^i \\ y_b^i \end{Bmatrix}, \quad u^i = \begin{Bmatrix} u_c^i \\ u_b^i \end{Bmatrix}. \tag{22}$$

For simplicity in this section, we let the coupling responses y_c^i be displacements. The synthesis is performed enforcing kinematic constraints and equilibrium conditions at the coupling DOFs. If the coupling DOFs of the two subsystems are co-oriented and numbered in the same order, the relation for response and excitation quantities between the uncoupled subsystem models and the synthesized model reads

$$\begin{Bmatrix} y_c^{\mathrm{I}} \\ y_c^{\mathrm{II}} \end{Bmatrix} = \begin{bmatrix} I \\ I \end{bmatrix} \bar{y}_c, \quad \bar{u}_c = \begin{bmatrix} I & I \end{bmatrix} \begin{Bmatrix} u_c^{\mathrm{I}} \\ u_c^{\mathrm{II}} \end{Bmatrix}, \tag{23}$$

where the bar indicate a synthesized model quantity. In order to obtain a minimal realization of the coupled subsystem model, constraints have also to be put on the state vectors x^i, $i = \mathrm{I}, \mathrm{II}$. It is well known that enforcement of n_c scalar kinematic constraints will reduce the total number of DOFs of the two subsystems by n_c. Hence in terms of a state-space model, the state vector of the coupled system $\bar{x}$ should have length $n^{\mathrm{I}} + n^{\mathrm{II}} - 2n_c$, where n^i is the length of x^i, $i = \mathrm{I}, \mathrm{II}$, cf. Su and Juang [13]. Therefore we introduce a state transformation $\tilde{x}^i = T^i x^i$ so that

$$\tilde{x}^i = T^i x^i = \begin{Bmatrix} \dot{y}_c^i \\ y_c^i \\ x_b^i \end{Bmatrix}. \tag{24}$$

With such a transformation it will be shown below that the state-space matrices transform into a particular structure called the coupling form as

$$\tilde{A}^i = \begin{bmatrix} A_{vv}^i & A_{vd}^i & A_{vb}^i \\ I & 0 & 0 \\ 0 & A_{bd}^i & A_{bb}^i \end{bmatrix}, \quad \tilde{B}^i = \begin{bmatrix} B_{vv}^i & B_{vb}^i \\ 0 & 0 \\ 0 & B_{bb}^i \end{bmatrix}, \quad \tilde{C}^i = \begin{bmatrix} 0 & I & 0 \\ C_{bv}^i & C_{bd}^i & C_{bb}^i \end{bmatrix}. \tag{25}$$

The synthesized state-space model describing the coupled system is then established on the corresponding structured form using Eqs. (23) and (25) as

$$\begin{Bmatrix} \ddot{\bar{y}}_c \\ \dot{\bar{y}}_c \\ \dot{x}_b^{\mathrm{I}} \\ \dot{x}_b^{\mathrm{II}} \end{Bmatrix} = \begin{bmatrix} \bar{A}_{vv} & \bar{A}_{vd} & \bar{A}_{vb}^{\mathrm{I}} & \bar{A}_{vb}^{\mathrm{II}} \\ I & 0 & 0 & 0 \\ 0 & A_{bd}^{\mathrm{I}} & A_{bb}^{\mathrm{I}} & 0 \\ 0 & A_{bd}^{\mathrm{II}} & 0 & A_{bb}^{\mathrm{II}} \end{bmatrix} \begin{Bmatrix} \dot{\bar{y}}_c \\ \bar{y}_c \\ x_b^{\mathrm{I}} \\ x_b^{\mathrm{II}} \end{Bmatrix} + \begin{bmatrix} \bar{B}_{vv} & \bar{B}_{vb}^{\mathrm{I}} & \bar{B}_{vb}^{\mathrm{II}} \\ 0 & 0 & 0 \\ 0 & B_{bb}^{\mathrm{I}} & 0 \\ 0 & 0 & B_{bb}^{\mathrm{II}} \end{bmatrix} \begin{Bmatrix} \bar{u}_c \\ u_b^{\mathrm{I}} \\ u_b^{\mathrm{II}} \end{Bmatrix}, \tag{26}$$

$$\begin{Bmatrix} \bar{y}_c \\ y_b^{\mathrm{I}} \\ y_b^{\mathrm{II}} \end{Bmatrix} = \begin{bmatrix} 0 & I & 0 & 0 \\ C_{bv}^{\mathrm{I}} & C_{bd}^{\mathrm{I}} & C_{bb}^{\mathrm{I}} & 0 \\ C_{bv}^{\mathrm{II}} & C_{bd}^{\mathrm{II}} & 0 & C_{bb}^{\mathrm{II}} \end{bmatrix} \begin{Bmatrix} \dot{\bar{y}}_c \\ \bar{y}_c \\ x_b^{\mathrm{I}} \\ x_b^{\mathrm{II}} \end{Bmatrix}. \tag{27}$$

With $K = (B_{vv}^{\mathrm{I}} + B_{vv}^{\mathrm{II}})^{-1}$, ($B_{vv}^{\mathrm{I}} + B_{vv}^{\mathrm{II}}$ assumed to be non-singular) the partitions are explicitly

$$\bar{A}_{vv} = B_{vv}^{\mathrm{I}} K \bar{A}_{vv}^{\mathrm{II}} + B_{vv}^{\mathrm{II}} K \bar{A}_{vv}^{\mathrm{I}}, \tag{28}$$

$$\bar{A}_{vd} = B_{vv}^{\mathrm{I}} K \bar{A}_{vd}^{\mathrm{II}} + B_{vv}^{\mathrm{II}} K \bar{A}_{vd}^{\mathrm{I}}, \tag{29}$$

$$\bar{A}_{vb}^{\mathrm{I}} = B_{vv}^{\mathrm{II}} K \bar{A}_{vb}^{\mathrm{I}}, \tag{30}$$

$$\bar{A}_{vb}^{\mathrm{II}} = B_{vv}^{\mathrm{I}} K \bar{A}_{vb}^{\mathrm{II}}, \tag{31}$$

$$\bar{B}_{vv} = B_{vv}^{\mathrm{I}} K B_{vv}^{\mathrm{II}}, \tag{32}$$

$$\bar{B}_{vb}^{\mathrm{I}} = B_{vv}^{\mathrm{II}} K B_{vb}^{\mathrm{I}}, \tag{33}$$

$$\bar{B}_{vb}^{\mathrm{II}} = B_{vv}^{\mathrm{I}} K B_{vb}^{\mathrm{II}}. \tag{34}$$

The state transformation matrices T^i resulting in a state-space model on coupling form is constructed in a two-step procedure as follows. The superscript i is dropped for convenience.

1. To initiate, setup a matrix T_0 and compute the inverse $Z_0 = T_0^{-1}$ where

$$T_0 = \begin{bmatrix} C_c A \\ C_c \\ N \end{bmatrix} \stackrel{\text{def}}{=} \begin{bmatrix} T_1 \\ T_2 \\ T_{0,3} \end{bmatrix}. \tag{35}$$

   Here N is an arbitrary selected subspace of the nullspace of B_c such that $NB_c = 0$ and T_0 is non-singular. B_c and C_c indicate the n_c first columns of B and rows of C, respectively.
2. The transformation matrix T is then established as

$$T = \begin{bmatrix} C_c A \\ C_c \\ N(I - AZ_{0,1}C_c) \end{bmatrix} \stackrel{\text{def}}{=} \begin{bmatrix} T_1 \\ T_2 \\ T_3 \end{bmatrix}, \tag{36}$$

   where $Z_{0,1}$ constitute the n_c first columns of Z_0 with $T_1 Z_{0,1} = I$ and the inverse of the transformation matrix is

$$Z = T^{-1} \stackrel{\text{def}}{=} \begin{bmatrix} Z_1 & Z_2 & Z_3 \end{bmatrix} \tag{37}$$

   with dimensions of Z_1, Z_2 and Z_3 consistent with the dimensions of T_1, T_2 and T_3 in Eq. (36) such that $T_1 Z_1 = I$, $T_2 Z_2 = I$ and $T_3 Z_3 = I$.

Lemma 3 (*Coupling form*). *The similarity transformation* $\tilde{A} = TAT^{-1}$, $\tilde{B} = TB$, $\tilde{C} = CT^{-1}$ *with T as defined by Eqs.* (35)–(37) *gives the state-space matrices* $\{\tilde{A}, \tilde{B}, \tilde{C}\}$ *on the coupling form according to Eq.* (25).

Proof. Using the identity $T_1 Z_{0,1} = T_1 Z_1 = I$, it is observed that $Z_1 = Z_{0,1}$. Then, consider the prescribed partitions of $\tilde{A}$ according to the coupling form equations (25). Evaluating the second row partition and using that $TZ = I$, we obtain

$$T_2 AZ = C_c AZ = T_1 Z = \begin{bmatrix} I & 0 & 0 \end{bmatrix}. \tag{38}$$

For the lower-left block of $\tilde{A}$ we have that

$$T_3 AZ_1 = N(AZ_{0,1} - AZ_{0,1} \underbrace{C_c AZ_{0,1}}_{=I}) = 0. \tag{39}$$

For the second row partition of $\tilde{B}$ we get

$$T_2 B = C_c B = 0 \tag{40}$$

provided that the model is consistent with Newton's second law. The product $C_c B$ corresponds to the direct throughput matrix relating force to velocity, but since no such relation exist, $C_c B = 0$ must hold. For the lower-left block of $\tilde{B}$ we have that

$$T_3 B_c = N(B_c - AZ_{0,1} \underbrace{C_c B_c}_{=0}) = NB_c = 0. \tag{41}$$

Finally for the first row partition of $\tilde{C}$ we obtain

$$C_c Z = T_2 Z = \begin{bmatrix} 0 & I & 0 \end{bmatrix} \tag{42}$$

which concludes the proof. □

The state-space model synthesis presented above requires that the models at least have to contain the input–output relation of loading and response between all interface DOFs. Consequently a test revealing their properties has to include excitation and response measurement at all interface DOFs, which in practice often is

cumbersome. Fortunately, the reciprocity property provides a possibility to circumvent this requirement under certain conditions. This is possible, since in theory, it is sufficient to have one collocated and co-orientated sensor–actuator pair anywhere in the structure and complementary sensing at the interface to obtain the required FRFs provided all system modes are controllable from the actuation.

Other approaches to measure FRFs for DOFs that have not been excited have been proposed. Different mass-loading techniques have been presented by Su and Juang [13], Ashory and Ewins [26] and Silva et al. [27]. For each non-excited interface DOF, translational or rotational, yet another measurement with a small rigid body, having well known mass and inertia properties, is attached to the structure at the specific interface DOF. This additional measurement was shown to provide sufficient information to calculate the unknown transfer function. In Silva et al. [28] a scheme based on this approach utilizing the mass-loading provided by the sensors themselves, usually accelerometers, was presented. Avitabile and O'Callahan [29] proposed a fundamentally different method relying on the system equivalent reduction/expansion process (SEREP). Using existing analytical or FE models of the structure under consideration a mapping between measured and unmeasured DOFs is developed.

4. Method verification

In order to verify the state-space model synthesis procedure, a simple numerical example is studied. Subsystem models identified from exact FRFs that are contaminated with artificial measurement noise are used. The FRFs of the resulting synthesized model of our method are then compared to the direct FRF synthesis technique by Jetmundsen et al. [8].

Two simple systems with discrete masses, springs and dashpots constitute the subsystems, see Fig. 1. The exact subsystem FRFs are constructed using the transfer function formulation for the second order equations of motion

$$H^i(\omega) = P_y^i(-\omega^2 M^i + \mathrm{i}\omega V^i + K^i)^{-1} P_u^i, \tag{43}$$

where $i = \mathrm{I}, \mathrm{II}$. The mass, viscous damping and stiffness matrices are

$$M^{\mathrm{I}} = \begin{bmatrix} m_1 & 0 & 0 \\ 0 & m_2 & 0 \\ 0 & 0 & m_3 \end{bmatrix}, \quad M^{\mathrm{II}} = \begin{bmatrix} m_4 & 0 & 0 \\ 0 & m_5 & 0 \\ 0 & 0 & m_6 \end{bmatrix}, \tag{44}$$

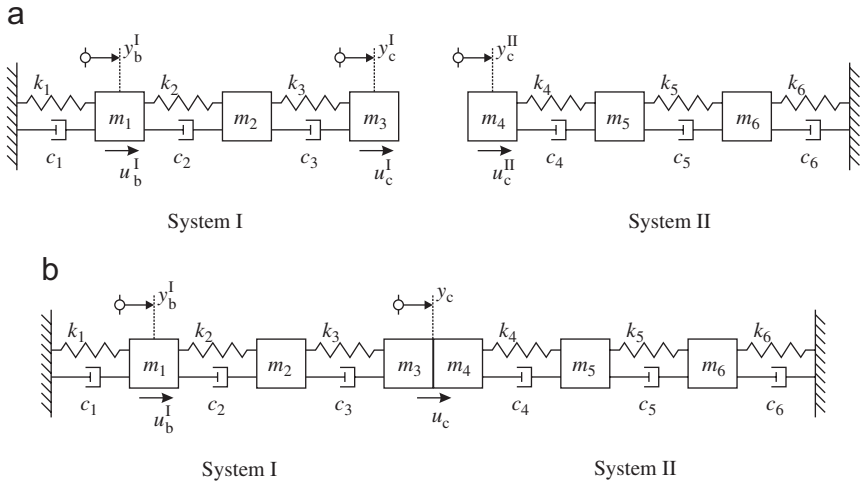

Fig. 1. (a) Uncoupled subsystems. (b) The coupled system.

$$V^{\mathrm{I}} = \begin{bmatrix} c_1 + c_2 & -c_2 & 0 \\ -c_2 & c_2 + c_3 & -c_3 \\ 0 & -c_3 & c_3 \end{bmatrix}, \quad V^{\mathrm{II}} = \begin{bmatrix} c_4 & -c_4 & 0 \\ -c_4 & c_4 + c_5 & -c_5 \\ 0 & -c_5 & c_5 + c_6 \end{bmatrix}, \tag{45}$$

$$K^{\mathrm{I}} = \begin{bmatrix} k_1 + k_2 & -k_2 & 0 \\ -k_2 & k_2 + k_3 & -k_3 \\ 0 & -k_3 & k_3 \end{bmatrix}, \quad K^{\mathrm{II}} = \begin{bmatrix} k_4 & -k_4 & 0 \\ -k_4 & k_4 + k_5 & -k_5 \\ 0 & -k_5 & k_5 + k_6 \end{bmatrix} \tag{46}$$

and the matrices of input and output coefficients for subsystems I and II are

$$P_y^{\mathrm{I}} = P_u^{\mathrm{I}\,T} = \begin{bmatrix} 0 & 0 & 1 \\ 1 & 0 & 0 \end{bmatrix}, \quad P_y^{\mathrm{II}} = P_u^{\mathrm{II}\,T} = \begin{bmatrix} 1 & 0 & 0 \end{bmatrix}. \tag{47}$$

The physical parameters have values according to Table 1.

Artificial measurement noise is introduced by perturbing the exact transfer function. The elements of the noisy FRF matrix at discrete frequencies ω_k are constructed as

$$H_{ij,m}(\omega_k) = H_{ij}(\omega_k) + \alpha_{ijk} + \mathrm{i}\beta_{ijk}, \tag{48}$$

where α_{ijk} and β_{ijk} are Gaussian distributed independent stochastic variables with zero mean and a standard deviation of 1×10^{-3} m/Ns. These noisy FRFs constitute the input to the system identification routines. Two versions of identified subsystem models are used in the state-space synthesis procedure, the models as identified by the subspace method, referred to as physically inconsistent models, and physically consistent models, where the subspace identified models have been modified to be physically consistent according to Sections 2.3 and 2.4.

In Table 2, the poles of the identified subsystem models compared to the exact subsystem poles are presented. In Figs. 2 and 3 some FRFs of the subsystems are shown. Notice that the phase angles of the direct point FRF in Fig. 2 of the physically inconsistent model lies outside the interval $[-90^\circ, 90^\circ]$, implying violation of the passivity constraint. In Fig. 4, FRFs of the coupled system model are compared to the corresponding exact FRF. The poles of the synthesized model are compared to the exact poles of the coupled system in

Table 1
Physical parameter values

i	m_i (kg)	c_i (Ns/m)	k_i (kN/m)
1	1.0	1.0	1.0
2	3.0	2.0	2.0
3	2.0	1.5	1.5
4	4.0	0.15	1.5
5	2.0	0.40	4.0
6	6.0	0.05	0.5

Table 2
Identified subsystem poles

Subsystem I		Subsystem II	
Identified poles	Exact poles	Identified poles	Exact poles
-0.0354 ± 10.7240i	-0.0572 ± 10.7003i	-0.0017 ± 6.2268i	-0.0019 ± 6.2274i
-0.6017 ± 34.9094i	-0.6093 ± 34.9024i	-0.0236 ± 21.9137i	-0.0240 ± 21.9141i
-1.7954 ± 59.9520i	-1.7918 ± 59.8365i	-0.1555 ± 58.0696i	-0.1678 ± 57.9307i

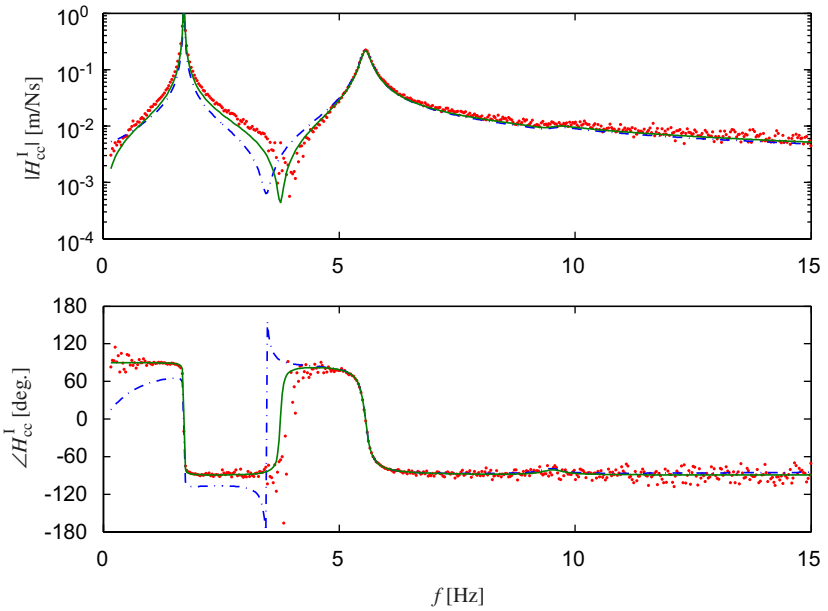

Fig. 2. Direct point mobility of subsystem I at the interface DOF. Artificial test data (dotted), physically inconsistent model (dash-dotted) and physically consistent model (solid).

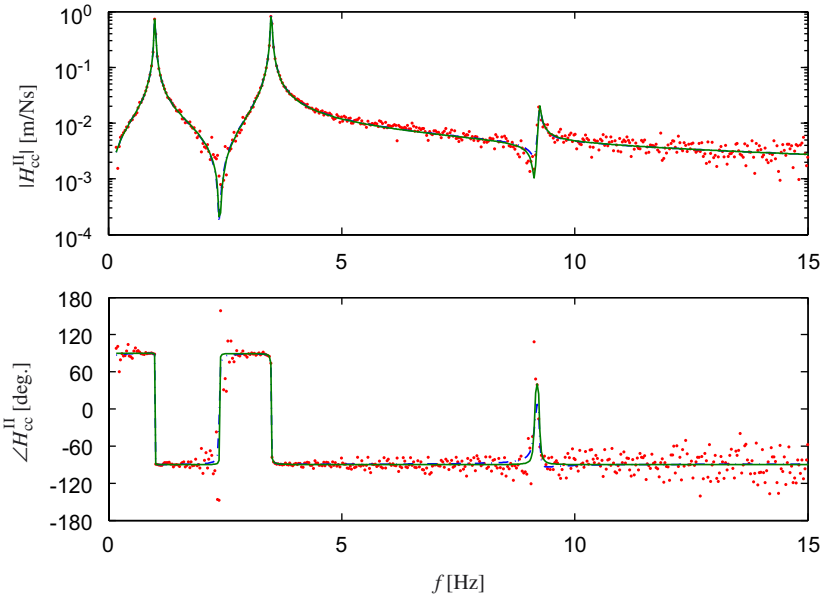

Fig. 3. Direct point mobility of subsystem II at the interface DOF. Artificial test data (dotted), physically inconsistent model (dash-dotted) and physically consistent model (solid). The dash-dotted and the solid curves almost coincide.

Table 3. It is observed that although both types of subsystem models capture the behaviour at subsystem level, only the physically consistent models gives reliable results after the assembly procedure. For the physically inconsistent subsystem models, some poles of the synthesized model have positive real part, meaning that the system's stability has been lost. It can be concluded that the use of physically consistent models serves as a regularization of that problem.

Table 3
Comparison of identified poles and exact poles of the coupled system

Physically inconsistent model	Physically consistent model	Exact poles
$0.0495 \pm 8.1953i$	$-0.0124 \pm 8.0069i$	$-0.0168 \pm 7.7744i$
$-0.4570 \pm 17.6455i$	$-0.0422 \pm 18.0127i$	$-0.0492 \pm 18.4312i$
$-1.1281 \pm 29.0976i$	$-0.3597 \pm 29.2805i$	$-0.3780 \pm 29.4611i$
$-0.1733 \pm 57.8752i$	$-0.1655 \pm 57.8518i$	$-0.1766 \pm 57.7222i$
$-1.8523 \pm 59.8973i$	$-1.7771 \pm 59.7980i$	$-1.7753 \pm 59.6935i$

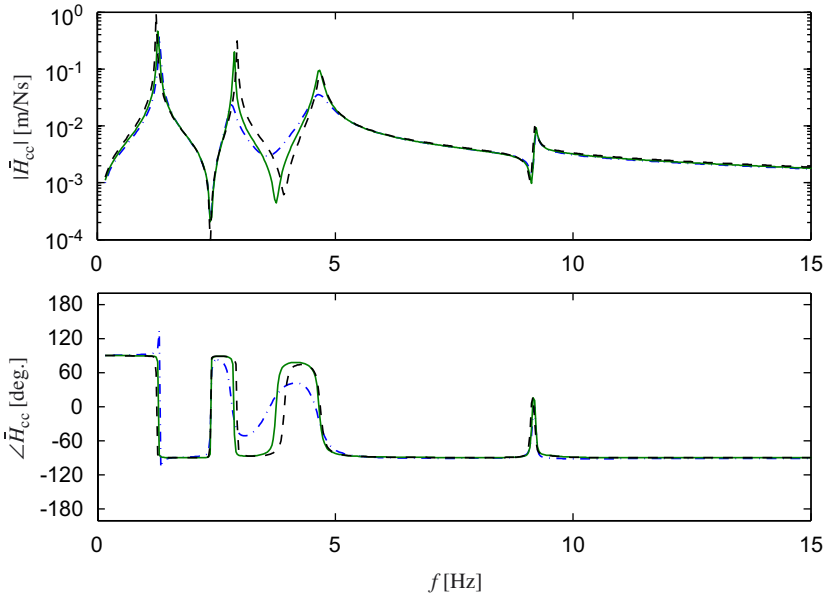

Fig. 4. Direct mobility of the coupled system at the interface DOF. Synthesis of physically inconsistent subsystem models (dash-dotted) and of physically consistent subsystem models (solid), compared to the exact FRFs (dashed).

Also the FRF coupling scheme according to Jetmundsen et al. [8] have been employed for comparison, see Fig. 5. It is observed that scatter occurs around the resonance peaks.

5. Case study

The outlined synthesis procedure was applied to a plane frame structure built from two subsystems that were rigidly connected at two points, giving in total four translational and two rotational coupling DOFs, see Fig. 6. Each subsystem was tested individually in a stepped sine test at every 0.25 Hz from 10 to 350 Hz. The outer frame, subsystem I, was excited with one single input force. The response was measured in the six coupling DOFs, at one additional location and in a DOF collocated and co-orientated with the excitation. The inner frame, subsystem II was excited in two DOFs and the response was measured in eight DOFs, the six coupling DOFs and in both of the excitation DOFs. Rotational motion was obtained by differentiation using two separated translational sensors.

State-space models of the two subsystems were identified using the frequency domain input–output data. The subspace method by McKelvey et al. [15] was used to estimate the system poles, i.e. the A-matrix. The model order determination was made using MIF plots, stabilization charts and qualitative FE models. The model order determined by FE analysis was checked by MIF analysis on experimental data and the pole

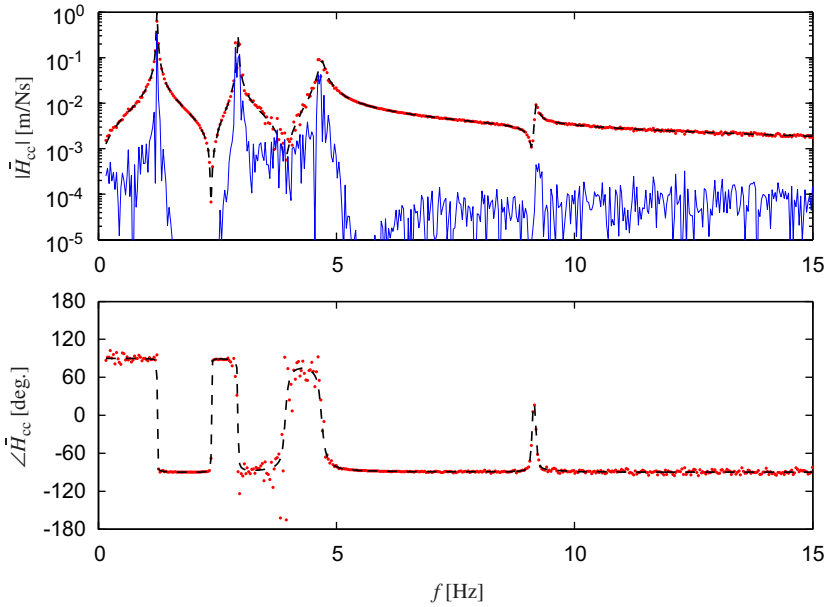

Fig. 5. Direct mobility of the coupled system at the interface DOF. FRF-based coupling according to Jetmundsen et al. [8] (dotted) compared to the exact FRFs (dashed) together with the deviation in magnitude (solid).

locations as obtained by stabilization charts. The method of considering experimental data only, by MIF analysis or others, was rejected since no clear order indication was obtained from available data. Then, the *B*- and *C*-matrices were established so that the models were physically consistent, see Sections 2.3 and 2.4. In Table 4 the eigenfrequencies of the identified models are compared to those of the FE models. The three lowest frequency modes of the FE models with eigenfrequencies below 10 Hz were included to the model as residual modes according to Section 2.4. In Figs. 7 and 8, FRFs are shown together with the FRFs of the identified state-space models and the corresponding FRFs of the FE models. The subsystem models were synthesized resulting in a coupled system model which was able to reproduce the test data with good accuracy, see Fig. 10.

In order to elucidate the importance of the subsystem model order, the case when the identified model of the outer frame, subsystem I, has been given an incorrect model order was considered. From the FE model two adjacent eigenfrequencies just above 70 Hz can be observed. The corresponding mode shapes describe the coupling elements (element A in Fig. 6) vibrating in-phase and out-of-phase with the rest of the structure practically in rest. The coupling elements are almost identical, thus these two eigenfrequencies are very close. Considering the measured data only, these modes could easily be mistaken as a single mode. Estimating the physically consistent *B*- and *C*-matrices corresponding to the lower order *A*-matrix of the outer frame provides a subsystem model that well reproduces the experimental data on subsystem level, see Fig. 9. However, the incorrect model order implies an identified subsystem model with constrained motion pattern. Consequently this will severely influence the synthesized model as is also visualized in Fig. 10.

6. Concluding remarks

A procedure for component synthesis using subsystem state-space models has been presented. Subsystem models identified from test data or based on first principles can be used to build the coupled system model, provided that the models describe the input–output behaviour between all interface DOFs. Regarding the system identification approach and testing, this requires that all interface DOFs and the excitation DOF are equipped with response sensors.

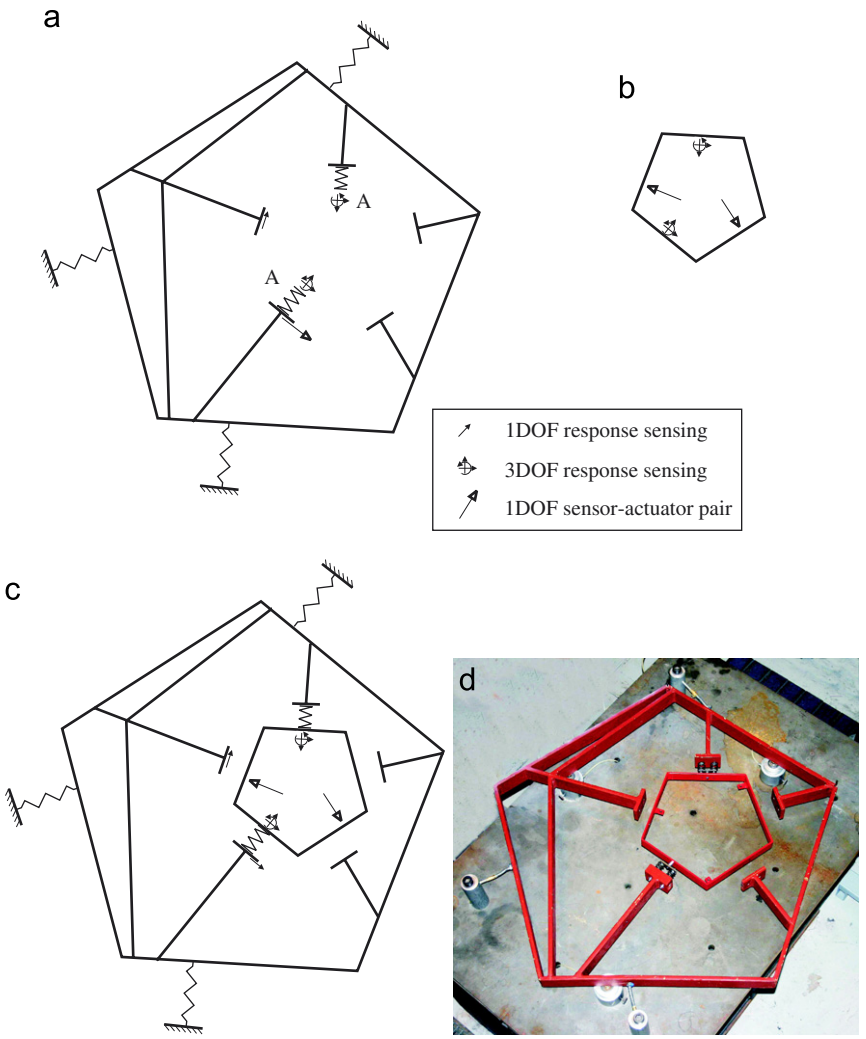

Fig. 6. Experimental test setup. (a) The outer frame with two helicoil spring coupling elements A. (b) The inner frame. (c,d) Coupled system.

In the system identification on substructure level, significant effort has to be put on model order determination and accurate estimation of low frequency residual modes outside the frequency range of interest. The subsystem synthesis is likely to fail unless all subsystem eigenmodes with eigenfrequencies below the upper frequency limit of the range of interest are included. Furthermore, we identify subsystem models that are physically consistent. A numerical example showed that synthesis of physically inconsistent state-space models with high-precision fit to experimental data may result in a coupled system model unable to describe the behaviour of the assembled structure. The use of models that do not violate basic physical properties can be regarded as a regularization of that problem.

When performing measurements on subsystem level, the test of the components should ideally be made with boundary conditions corresponding to those of the total system in normal operation. In practice this is not easily obtained since that may require component testing under pure free–free conditions. Any deviation from this ideal case would introduce systematic errors to the coupling procedure. In addition, test variability and measurement noise levels will influence the quality of the identified subsystem models and indirectly also the quality of the synthesized coupled system model. However, these aspects have not been explicitly investigated.

Table 4
Eigenfrequencies below 350 Hz of the subsystem models

Subsystem I		Subsystem II	
Identified model	FE model	Identified model	FE model
–	0.9235	–	0.0283
–	1.0968	–	0.0293
–	1.1979	–	0.1351
20.6657	19.5913	61.0366	60.4210
30.0545	28.4092	61.0456	60.5319
41.6136	43.5050	178.2310	178.0811
49.4380	49.7445	178.6576	179.2412
51.5510	52.4315	296.1711	293.9168
60.6767	60.2981	297.1078	295.3313
67.9527	66.3877	313.7049	306.3738
71.1862	71.7052		
71.8081	72.9175		
81.9893	81.2473		
100.2995	100.7438		
115.2624	116.0820		
124.2535	123.8303		
127.0144	128.9306		
135.0932	134.1356		
138.5848	135.6091		
161.3266	157.2672		
178.3872	175.0524		
194.5053	189.4426		
211.6879	213.3731		
217.9374	215.8197		
264.4583	263.3280		
267.4615	273.9547		
292.3606	305.4419		
316.7870	322.4421		

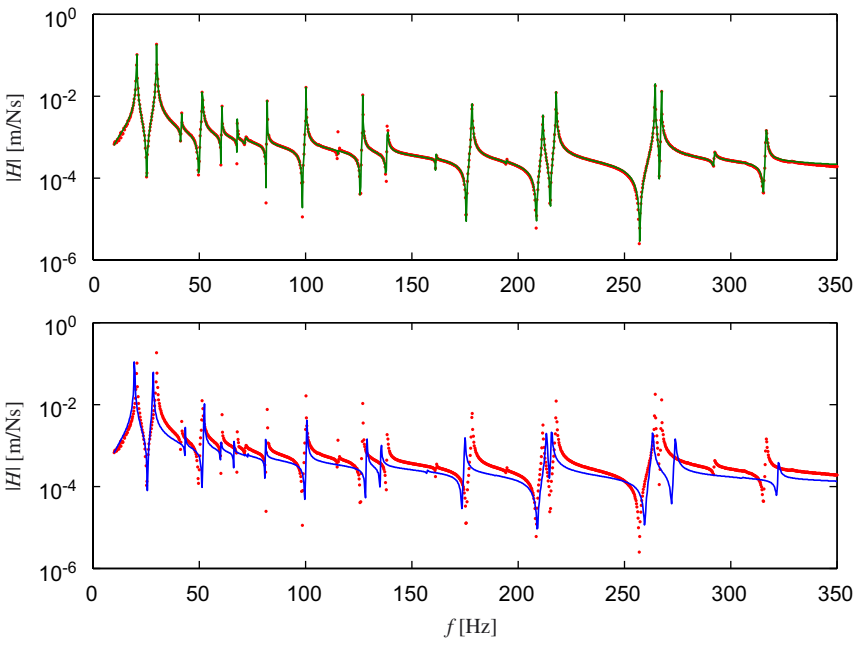

Fig. 7. Magnitude of the direct point mobility of the outer frame. Upper graph: identified model (solid) vs. measured FRF (dotted). Lower graph: FE model (solid) vs. measured FRF (dotted).

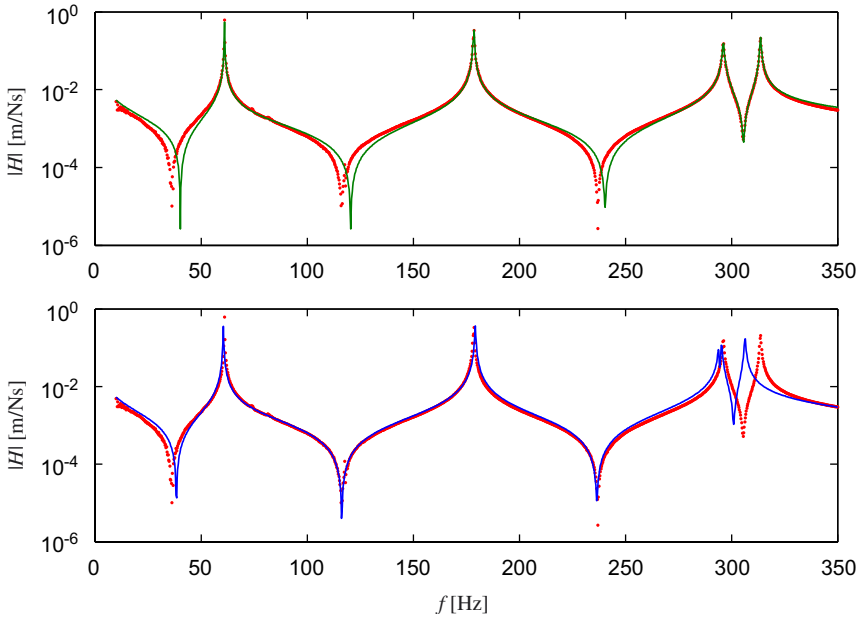

Fig. 8. Magnitude of a direct point mobility of the inner frame. Upper graph: identified model (solid) vs. measured FRF (dotted). Lower graph: FE model (solid) vs. measured FRF (dotted).

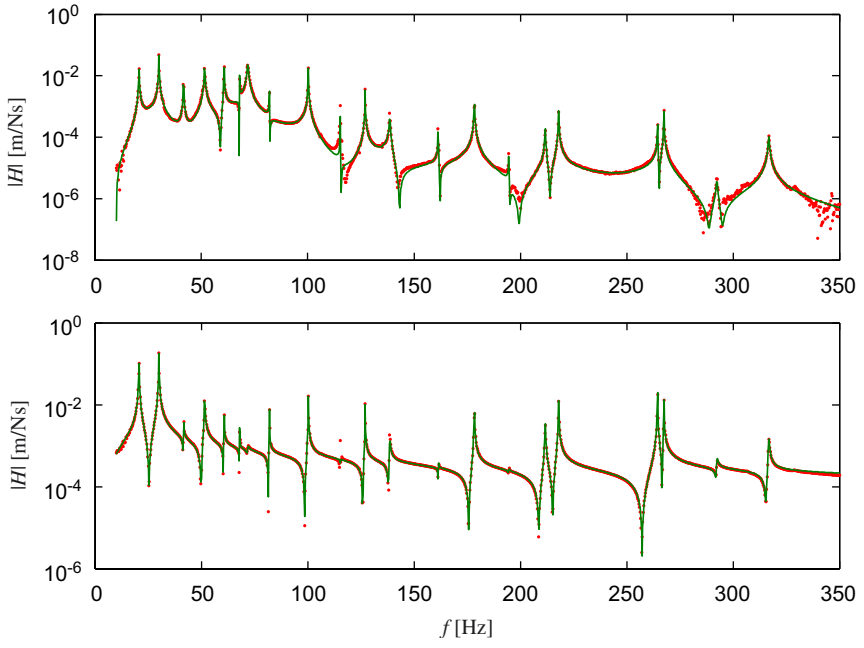

Fig. 9. Identified model of the outer frame with *incorrect* model order (solid) vs. experimental data (dotted). Upper graph: transfer mobility, the excitation DOF to a coupling DOF. Lower graph: direct point mobility, cf. Fig. 7.

The approach was applied to an example with real test data. Two plane frame structures were tested individually and physically consistent subsystem state-space models were identified. The models were synthesized resulting in a coupled system model that was able to reproduce test data of the assembled structure with good accuracy.

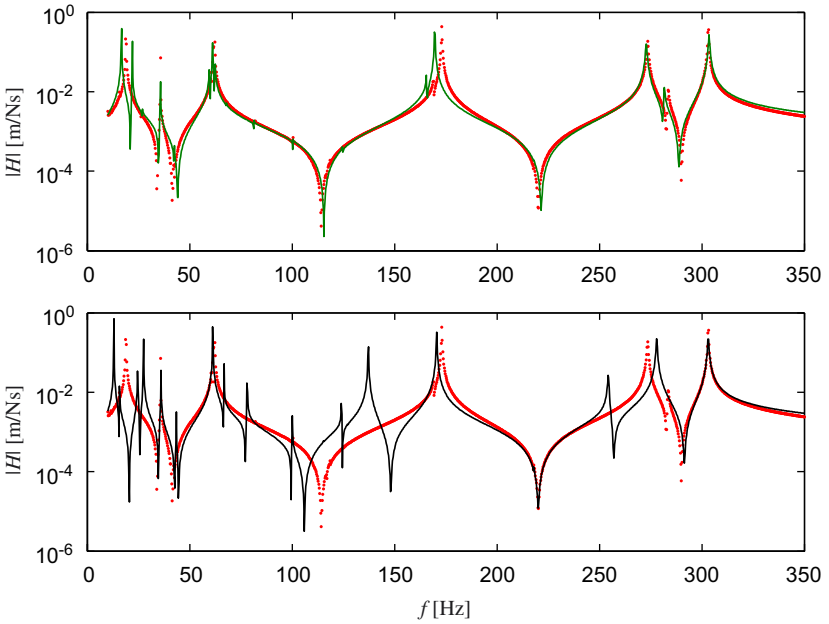

Fig. 10. Magnitude of a direct point mobility of the coupled system. Upper graph: synthesized model (solid) vs. measured FRF (dotted). Lower graph: synthesis using subsystem model with incorrect model order (solid) vs. measured FRF (dotted).

Acknowledgements

The authors gratefully acknowledge the supervision and support from Associate Professor Tomas McKelvey at the Department of Signals and Systems and the contribution from Mr. Hans Johansson at the Department of Applied Mechanics, both at Chalmers University of Technology. The work was performed within the Centre of Excellence CHARMEC (CHAlmers Railway MEChanics).

References

[1] L. Ljung, System Identification—Theory for the User, second ed., Prentice-Hall PTR, Upper Saddle River, NJ, 1999.
[2] M.I. Friswell, J.E. Mottershead, Finite Element Model Updating in Structural Dynamics, Kluwer Academic Publishers, Dordrecht, The Netherlands, 1995.
[3] D.J. Ewins, Modal Testing—Theory, Practice and Application, second ed., Research Studies Press Ltd., Baldock, Hertfordshire, England, 2000.
[4] L. Meirovitch, Computational Methods in Structural Dynamics, Sijthoff & Nordhoff, Alphen aan den Rijn, The Netherlands, 1980.
[5] R.R. Craig Jr., A brief tutorial on substructure synthesis and testing, in: Proceedings of the 18th International Modal Analysis Conference, 2000, pp. 899–908.
[6] R.R. Craig Jr., A.J. Kurdila, Fundamentals of Structural Dynamics, Wiley, Hoboken, NJ, 2006.
[7] R.E.D. Bishop, D.C. Johnson, The Mechanics of Vibration, Cambridge University Press, Cambridge, 1960.
[8] B. Jetmundsen, R.L. Bielawa, W.G. Flanelly, Generalized frequency domain substructure synthesis, Journal of the American Helicopter Society 33 (1988) 55–64.
[9] W. Liu, D.J. Ewins, Substructure synthesis via elastic media, Journal of Sound and Vibration 257 (2) (2002) 361–379.
[10] D. Otte, J. Leuridan, H. Grangier, R. Aquilina, Coupling of substructures using measured FRFs by means of SVD-based data reduction techniques, in: Proceedings of the Eighth International Modal Analysis Conference, 1990, pp. 213–220.
[11] T.C. Lim, J. Li, A theoretical and computational study of the FRF-based substructuring technique applying enhanced least square and TSVD approaches, Journal of Sound and Vibration 231 (4) (2000) 1135–1157.
[12] Y. Ren, C.F. Beards, On substructure synthesis with FRF data, Journal of Sound and Vibration 185 (5) (1995) 845–866.
[13] T.-J. Su, J.-N. Juang, Substructure system identification and synthesis, Journal of Guidance, Control and Dynamics 17 (5) (1994) 1087–1095.
[14] P. Van Overschee, B. DeMoor, Subspace Identification of Linear Systems: Theory Implementations, Applications, Kluwer Academic Publishers, Boston, MA, 1996.

[15] T. McKelvey, H. Akçay, L. Ljung, Subspace-based multivariable system identification from frequency response data, IEEE Transactions on Automatic Control 41 (7) (1996) 960–979.
[16] M. Viberg, Subspace-based state-space system identification, Circuits, Systems and Signal Processing 21 (1) (2002) 23–37.
[17] M. Radeş, A comparison of some mode indicator functions, Mechanical Systems and Signal Processing 8 (4) (1994) 459–474.
[18] B. Cauberghe, P. Guillaume, P. Verboven, S. Vanlanduit, E. Parloo, On the influence of the parameter constraint on the stability of poles and the discrimination capabilities of the stabilisation diagrams, Mechanical Systems and Signal Processing 19 (2005) 989–1014.
[19] L. Meirovitch, Principles and Techniques of Vibrations, Prentice-Hall, Upper Saddle River, NJ, 1997.
[20] P. Sjövall, T. McKelvey, T. Abrahamsson, Constrained state-space system identification with application to structural dynamics, Automatica 42 (2006) 1539–1546.
[21] B.D.O. Anderson, S. Vongpanitlerd, Network Analysis and Synthesis, Prentice-Hall, Englewood Cliffs, NJ, 1973.
[22] K.J. Åström, B. Wittenmark, Adaptive Control, Addison-Wesley, Reading, MA, 1989.
[23] R.F. Curtain, Old and new perspectives on the positive-real lemma in systems and control theory, Zeitschrift fur Angewandte Mathematik und Mechanik 79 (9) (1999) 579–590.
[24] B.D.O. Anderson, A system theory criterion for positive real lemma matrices, SIAM J. Control 5 (2) (1967) 171–182.
[25] K.F. Alvin, K.C. Park, Second-order structural identification procedure via state-space-based system identification, AIAA Journal 32 (2) (1994) 397–406.
[26] M.R. Ashory, D.J. Ewins, Generations of the whole FRF matrix from measurements on one column, in: Proceedings of the 16th International Modal Analysis Conference, 1998, pp. 800–814.
[27] J.M.M. Silva, N.M.M. Maia, A.M.R. Ribiero, Indirect measurement of rotational frequency response functions in: Proceedings of the 19th International Modal Analysis Conference, 2001, pp. 1535–1542.
[28] J.M.M. Silva, N.M.M. Maia, A.M.R. Ribiero, Cancellation of mass-loading effects of transducers and evaluation of unmeasured frequency response functions, Journal of Sound and Vibration 236 (5) (2000) 761–779.
[29] P. Avitabile, J. O'Callahan, Frequency response function expansion for unmeasured translation and rotation DOFs for impedance modelling applications, Mechanical Systems and Signal Processing 17 (4) (2003) 723–745.